



Limits on Anomalous $WW\gamma$ Couplings from $p\bar{p} \rightarrow W\gamma X$ Events at $\sqrt{s} = 1.96$ TeV

The DØ Collaboration
URL <http://www-d0.fnal.gov>
(Dated: February 2, 2005)

The $WW\gamma$ triple gauge boson coupling parameters are studied using $p\bar{p} \rightarrow \ell\nu\gamma X$ ($\ell = e, \mu$) events at $\sqrt{s} = 1.96$ TeV collected with the DØ detector from an integrated luminosity of 162.3 pb^{-1} delivered by the Fermilab Tevatron Collider. The cross section times branching ratio for $p\bar{p} \rightarrow W(\gamma)X \rightarrow \ell\nu\gamma X$ with $E_T^\gamma > 8 \text{ GeV}$ and $\Delta\mathcal{R}_{\ell\gamma} > 0.7$ is measured to be $14.8 \pm 1.6(\text{stat}) \pm 1.0(\text{sys}) \pm 1.0(\text{lumi}) \text{ pb}$. The one dimensional 95% confidence level limits on anomalous couplings are $-0.93 < \Delta\kappa_\gamma < 0.97$ and $-0.22 < \lambda_\gamma < 0.22$.

I. INTRODUCTION

The $W\gamma$ final states observed at hadron colliders provide an opportunity to study the self-interaction of electroweak bosons at the $WW\gamma$ vertex. The Standard Model (SM) description of electroweak physics is based on $SU(2)_L \otimes U(1)_Y$ gauge theory and specifies the $WW\gamma$ coupling. In order to allow for non-standard coupling, a CP-conserving effective Lagrangian can be written with two coupling parameters: κ_γ and λ_γ [1, 2]. The SM predicts $\Delta\kappa_\gamma = \kappa_\gamma - 1 = 0$ and $\lambda_\gamma = 0$. Non-standard couplings cause the effective Lagrangian to violate partial wave unitarity at high energies; it is necessary to introduce form factors with scale Λ for each of the coupling parameters. The form factors are introduced through substitutions of the form $\lambda \rightarrow \lambda/(1 + \hat{s}/\Lambda^2)^2$ with \hat{s} the $W\gamma$ invariant mass and Λ set to 1.5 TeV for this analysis. Deviations from the SM $WW\gamma$ couplings would cause an increase in the total $W\gamma$ production cross section, and would enhance the production of photons with high transverse energy.

Limits on the $WW\gamma$ coupling parameters have been previously reported by CDF and DØ using direct observation of $W\gamma$ final states in data collected from hadron collisions at the Tevatron [3, 4] and by UA2 using the $S\bar{p}\bar{p}S$ collider [5]. Experiments at LEP constrain the $WW\gamma$ and WWZ coupling parameters simultaneously through observations of W^+W^- , single- W boson and single- γ final states in electron-positron collisions [6]. Observation of $b \rightarrow s\gamma$ decays at CLEO has also been used to constrain the coupling parameters [7].

II. EVENT SELECTION

The analyses discussed here use the DØ detector to observe $p\bar{p} \rightarrow \ell\nu\gamma X$ ($\ell = e$ or μ) events in collisions with $\sqrt{s} = 1.96$ TeV at the Fermilab Tevatron. The data samples used for the electron and muon channels correspond to integrated luminosities of 162.3 pb^{-1} and 134.4 pb^{-1} , respectively. The DØ detector [8] features an inner tracker surrounded by a liquid-argon/uranium calorimeter and a muon spectrometer. The inner tracker consists of a silicon microstrip tracker (SMT) and a central fiber tracker (CFT), both located within a 2 T superconducting solenoidal magnet. The CFT covers $|\eta| = |-\ln \tan(\theta/2)| < 1.8$ and the SMT covers $|\eta| < 3.0$. The calorimeter is housed in three cryostats: a central section covering $|\eta| < 1.1$ and two end-cap cryostats which extend coverage to $|\eta| < 4.0$. The muon detectors reside outside the calorimeter and consist of tracking detectors, scintillation trigger counters and a 1.8 T toroidal magnet. The muon detectors cover $|\eta| < 2.0$. Luminosity is measured using scintillator arrays located in front of the end-cap cryostats ($2.7 < |\eta| < 4.4$).

Candidate events with electron decays of the W boson ($W \rightarrow e\nu$) are collected using a suite of single electron triggers that require electromagnetic clusters in the calorimeter with at least 11 GeV of transverse energy (E_T). Offline electron identification requires the candidate objects to be in the central calorimeter ($|\eta| < 1.1$), isolated in the calorimeter, have shower shapes consistent with electromagnetic objects and have a track found in the inner tracker matched to the calorimeter cluster. Similarly, photons are identified as central electromagnetic calorimeter clusters without a matched track that are isolated both in the calorimeter and in the tracking detectors. In order to suppress events with final state radiation of the photon from the outgoing lepton, and to avoid collinear singularities in calculations, the photon is required to be separated from the electron in $\eta - \phi$ space ($\Delta\mathcal{R} = \sqrt{(\Delta\eta)^2 + (\Delta\phi)^2} > 0.7$). Events used in this analysis are required to have $E_T^e > 25$ GeV, $E_T^\gamma > 8$ GeV, missing transverse energy $\cancel{E}_T > 25$ GeV and $M_T > 40$ GeV/ c^2 , where M_T is the transverse mass $\sqrt{2E_T^e \cancel{E}_T (1 - \cos \phi^{e\nu})}$ of the electron and \cancel{E}_T vectors which are separated by $\phi^{e\nu}$ in azimuth.

Candidate events with muon decays of the W boson ($W \rightarrow \mu\nu$) are collected using a suite of single muon triggers that require a high p_T track in the muon detectors and a high p_T track in the central tracking detectors. Offline muon identification additionally restricts muon candidates to the central tracking volume ($|\eta| < 1.6$), requires matched central tracks, and imposes timing cuts to reduce backgrounds from cosmic and beam halo muons. Events with more than one identified muon are rejected to reduce backgrounds from $Z \rightarrow \mu\mu(\gamma)$. Photon identification in this analysis is the same as in the electron channel described above. The events used are required to have $p_T^\mu > 20$ GeV/ c , $E_T^\gamma > 8$ GeV, and $\cancel{E}_T > 20$ GeV.

III. BACKGROUND ESTIMATION

The dominant background for both decay channels is W +jet production where a jet mimics a photon. The contribution of this background is estimated by using a large multijet data sample to measure the fraction of jets that mimic photons. A fraction of multijet events contains true photons, and the fraction has previously been seen to increase with increasing transverse energy as $1 - e^{-a+bE_T}$ [9]. The systematic uncertainty on the probability of a jet being misidentified as a photon is conservatively taken to be the full difference between ignoring the presence of true photons in the

TABLE I: Summary of estimated backgrounds and numbers of events selected in each channel.

	Electron Channel	Muon Channel
Luminosity	162 pb ⁻¹	134 pb ⁻¹
W + jet Background Events	58.7 ± 4.5	61.8 ± 5.1
ℓeX Background Events	1.7 ± 0.5	0.7 ± 0.2
$W\gamma \rightarrow \tau\nu\gamma$ Background Events	0.42 ± 0.02	1.9 ± 0.2
$Z\gamma \rightarrow \ell\ell\gamma$ Background Events	-	6.9 ± 0.7
Total Background Events	60.8 ± 4.5	71.3 ± 5.2
Selected Events	112	161
Total Signal Events	51.2 ± 11.5	89.7 ± 13.7

multijet data sample and estimating their contribution with the above functional form. The probability of a jet mimicking a photon as a function of jet transverse energy is found to be $P(E_T) = (5.24 \pm 0.41) \times 10^{-3} - (5.9 \pm 1.2) \times 10^{-5} E_T$. The method described above is dependent on the jet energy scale; as a check of the accuracy of the jet energy scale the method is repeated using jet-like objects that have a high fraction of calorimeter energy in the electromagnetic layers. This yields a background estimate consistent with the method based on jets.

A second class of background events comes from processes which produce an electron or muon, an electron which is misidentified as a photon and missing transverse energy. This background, labeled ℓeX , is small for the muon channel since very few processes produce a high E_T muon and a high E_T electron. However, this background is significant for the electron channel since $Z \rightarrow ee$ + jet processes have a relatively large cross section. In order to reduce this background, an additional cut on the invariant mass of the electron and photon candidates is imposed and events with $70 < M_{e\gamma} < 110$ GeV/ c^2 are rejected. In both the electron and muon analyses, the ℓeX background is estimated by reversing the track match requirement on the photon candidate (*i.e.* require a matched track) in $W\gamma$ candidate events. The number of ℓeX events where the electron is both isolated and does not have a matched track (and therefore is misidentified as a photon) is then estimated using the known track matching and track isolation inefficiencies.

Small backgrounds from $Z\gamma$ and $W \rightarrow \tau\nu\gamma$ are estimated from Monte Carlo samples. The background estimates and numbers of events observed in the data are summarized in Table I.

IV. EFFICIENCY ESTIMATION

The efficiencies of the triggers and lepton identification cuts are measured using $Z \rightarrow ee, \mu\mu$ events. The efficiencies for electrons are 0.96 ± 0.02 for the trigger, 0.84 ± 0.01 for the calorimeter identification requirements and 0.78 ± 0.01 for the track match requirement. For muons, the trigger efficiency is 0.74 ± 0.01 , the offline reconstruction efficiency is 0.77 ± 0.02 and the efficiency of the track match requirement is 0.98 ± 0.01 . The efficiency of requiring no more than one muon in muon candidate events is estimated to be 0.942 ± 0.004 by counting the fraction of $Z \rightarrow ee$ events containing a muon. The track isolation efficiency used for the ℓeX background estimation is measured in $Z \rightarrow ee$ events and is found to be 0.95 ± 0.01 . The efficiency of the calorimeter requirements in photon identification are estimated using GEANT [10] to simulate the detector. The probability for unrelated tracks to overlap the photon and cause it to fail the track isolation requirements is measured in $Z \rightarrow ee$ events by measuring the probability of an electron to have nearby tracks after the event is rotated in ϕ by ninety degrees. The overall efficiency for photon identification is found to be 0.81 ± 0.01 . The total efficiencies are 0.51 ± 0.02 for the electron channel and 0.43 ± 0.01 for the muon channel.

The acceptances due to the kinematic and geometric requirements in the analyses are calculated using a Monte Carlo generator [2] that fully models $W\gamma$ production at leading order and allows anomalous coupling values to be set. The detector response is simulated using a fast parametric Monte Carlo. The effects of higher order QCD processes are accounted for by the introduction of a k -factor of 1.335 [2]. The CTEQ6L parton distribution function (PDF) [11] is used for the proton and anti-proton, and the transverse momentum spectrum of the W boson is simulated by PYTHIA [12]. The acceptances are determined to be 0.045 ± 0.002 for the electron channel and 0.102 ± 0.003 for the muon channel with the uncertainties dominated by the PDF uncertainty.

V. CROSS SECTIONS

The measured cross sections times branching ratios $\sigma(p\bar{p} \rightarrow W(\gamma)X \rightarrow \ell\nu\gamma X)$ with $E_T^\gamma > 8$ GeV and $\Delta\mathcal{R}_{\ell\gamma} > 0.7$ are $13.9 \pm 2.9 \pm 1.6 \pm 0.9$ pb for the electron channel and $15.2 \pm 2.0 \pm 1.1 \pm 1.0$ pb for the muon channel. Three

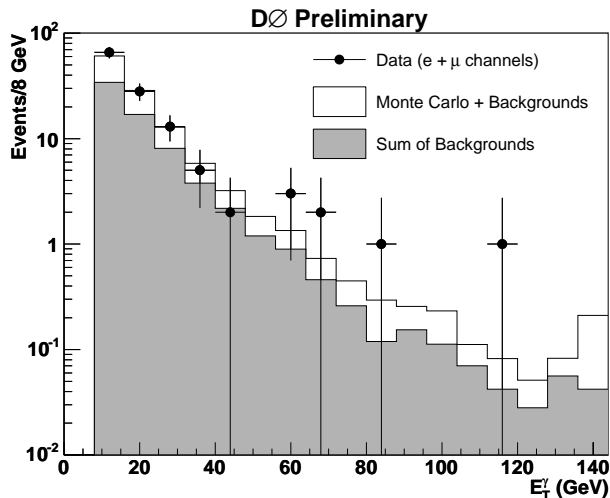


FIG. 1: The photon E_T spectrum for the $W\gamma$ candidates with $M_T(W, \gamma) > 90$ GeV. The points with error bars are the data. The open histogram is the sum of the SM Monte Carlo prediction and the background estimate (shown as the shaded histogram). The right-most bin shows the numbers of events for all events with photon E_T above 136 GeV.

components that contribute to the estimated cross section uncertainty are given separately; they are, in the order given: statistics; systematic effects associated with the background subtraction, acceptance calculation, and object identification; and systematic effects inherent in the luminosity measurement. When the two decay channels are combined, the cross section times branching ratio is measured to be $14.8 \pm 1.6 \pm 1.0 \pm 1.0$ pb. The SM prediction using CTEQ6L is 16.0 ± 0.4 pb, where the uncertainty is due to the parton distribution function uncertainty. The prediction is in agreement with the measurements.

VI. ANOMALOUS COUPLING LIMITS

The photon E_T spectrum of the candidate events is shown with the background estimation and the Standard Model expectations in Fig. 1. The distribution is described well by the Standard Model, and no enhancement of the photon E_T spectrum is seen at high transverse energy. Limits on anomalous couplings are determined by performing a binned likelihood fit to the photon E_T spectrum. The effect of anomalous couplings is more pronounced at high $W - \gamma$ transverse mass, $M_T(W, \gamma)$, so only events with $M_T(W, \gamma) > 90$ GeV are used for the distributions in the likelihood fit. Monte Carlo distributions of the photon E_T spectrum are generated with a range of anomalous coupling values, and the likelihood of the data distribution being consistent with the generated distribution is calculated. The uncertainties in the background estimates, efficiencies, acceptances and the luminosity are included in the likelihood calculation using Gaussian distributions.

Likelihood contours are shown in Fig. 2, with the contours showing the one- and two-dimensional 95% confidence level limits for the CP conserving coupling parameters. The one-dimensional limits on each parameter are $-0.93 < \Delta\kappa_\gamma < 0.97$ and $-0.22 < \lambda_\gamma < 0.22$, where the limit on λ_γ assumes $\Delta\kappa_\gamma$ is fixed to the Standard Model value and vice versa.

VII. SUMMARY

In summary, the cross section times branching ratio for the process $p\bar{p} \rightarrow W(\gamma)X \rightarrow \ell\nu\gamma X$ with $E_T^\gamma > 8$ GeV and $\Delta\mathcal{R}_{\ell\gamma} > 0.7$ is measured to be $14.8 \pm 1.6 \pm 1.0 \pm 1.0$ pb using 162.3 pb^{-1} of integrated luminosity delivered to the D0 detector during Run II of the Tevatron. The measured cross section is in agreement with the SM expectation of 16.0 ± 0.4 . Limits at the 95% confidence level on anomalous $WW\gamma$ couplings are calculated using the photon transverse energy spectrum and are found to be $-0.93 < \Delta\kappa_\gamma < 0.97$ and $-0.22 < \lambda_\gamma < 0.22$. These limits represent

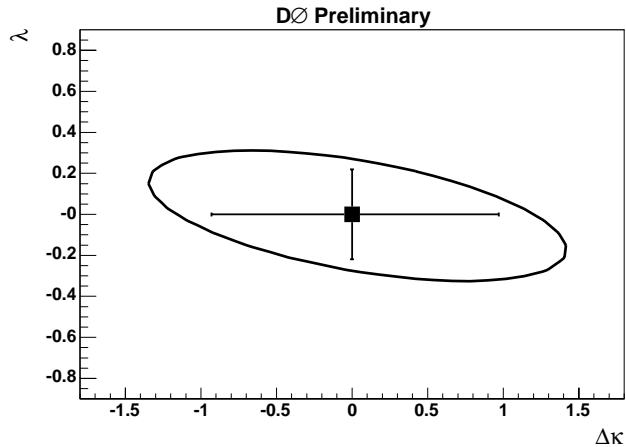


FIG. 2: Limits on the $WW\gamma$ coupling parameters $\Delta\kappa_\gamma$ and λ_γ . The point indicates the SM value with the error bars being the 95% confidence level intervals in one-dimension. The ellipse represents the two-dimensional 95% confidence level exclusion contour.

the most stringent constraints on anomalous $WW\gamma$ couplings obtained by direct observation of $W\gamma$ production.

-
- [1] K. Hagiwara *et al.*, Nucl. Phys. **B282**, 253 (1987).
 - [2] U. Baur and E. L. Berger, Phys. Rev. D **41**, 1476 (1990).
 - [3] DØ Collaboration, S. Abachi *et al.*, Phys. Rev. Lett. **78**, 3634 (1997).
 - [4] CDF Collaboration, F. Abe *et al.*, Phys. Rev. Lett. **75**, 1017 (1995); CDF Collaboration, D. Acosta *et al.*, arXiv:hep-ex/0410008.
 - [5] UA2 Collaboration, J. Alitti *et al.*, Phys. Lett. B **277**, 194 (1992).
 - [6] LEP Electroweak Working Group, U. Parzefall *et al.*, LEPEWWG/TGC/2003-01.
 - [7] CLEO Collaboration, M. S. Alam *et al.*, Phys. Rev. Lett. **74**, 2885 (1995).
 - [8] T. LeCompte and H.T. Diehl, Ann. Rev. Nucl. Part. Sci. **50**, 71 (2000).
 - [9] DØ Collaboration, S. Abachi *et al.*, Phys. Rev. Lett. **77**, 5011 (1996).
 - [10] R. Brun *et al.*, CERN-DD-78-2-REV.
 - [11] CTEQ Collaboration, J. Pumplin *et al.*, JHEP **0207**, 012 (2002); CTEQ Collaboration, D. Stump *et al.*, JHEP **0310**, 046 (2003).
 - [12] T. Sjöstrand *et al.*, Comp. Phys. Commun. **135**, 238 (2001).

APPENDIX

The transverse mass, three body mass, and photon-lepton charge signed rapidity difference for each channel are shown in Figures 3-8. Interference between photons produced from a $WW\gamma$ vertex and photons produced from initial state radiation is expected to cause the charge signed rapidity difference distribution to display a suppression of photons produced with $\Delta\eta \sim 0$. This suppression is known as a radiation amplitude zero. In the electron channel, the restriction of both electron and photon to the central calorimeter restricts the range of rapidity difference, eliminating any expected dip from interference. Since the muon channel is not as restricted, it does not suffer as greatly from the photon rapidity cuts. With the current statistics and fiducial requirements, it is not possible to determine that the behavior observed is Standard Model radiation amplitude zero. However, with the ability to identify forward photons and electrons ($|\eta| < 2.5$), it is expected that the radiation amplitude zero will be observable.

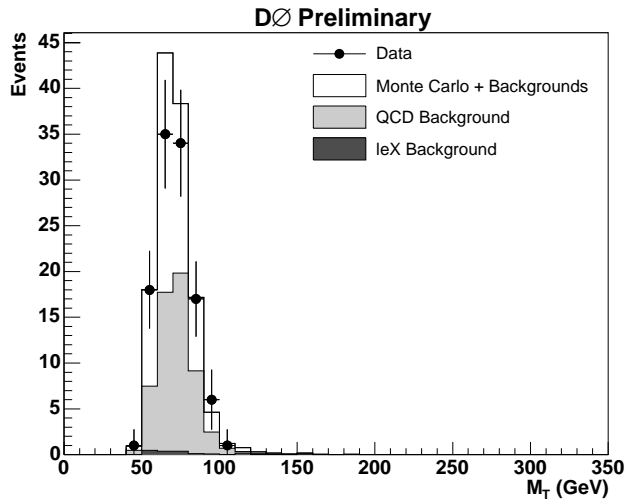


FIG. 3: Comparison of data (points), background (shaded histogram), and Monte Carlo + background (open histogram) for the transverse mass, M_T , in the $W(\gamma)X \rightarrow e\nu\gamma X$ analysis.

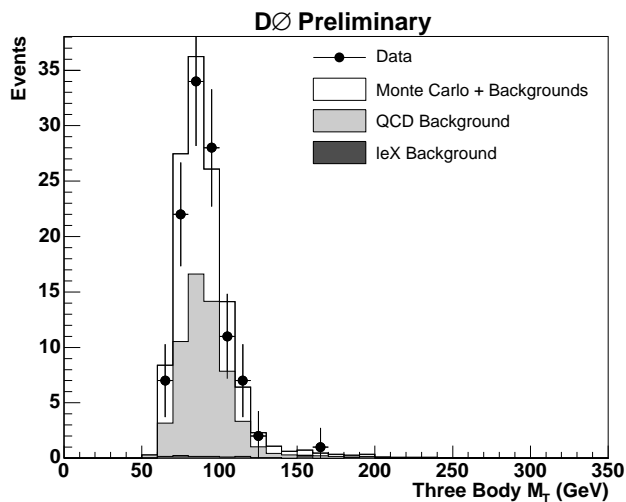


FIG. 4: Comparison of data (points), background (shaded histogram), and Monte Carlo + background (open histogram) for the threebody ($e\nu\gamma$) transverse mass in the $W(\gamma)X \rightarrow e\nu\gamma X$ analysis.

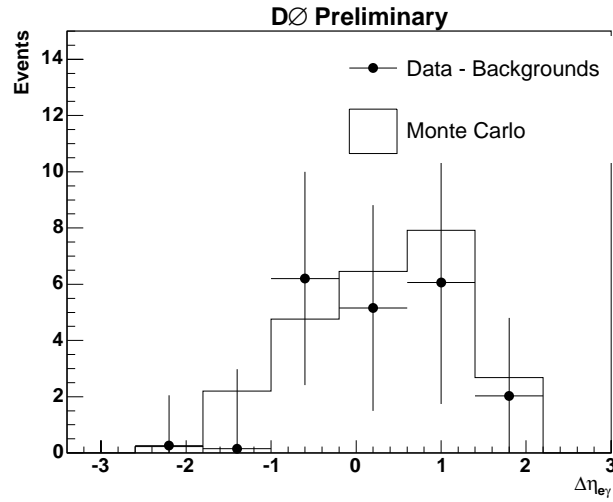


FIG. 5: Charge Signed Rapidity difference in electron channel. The background subtracted data is denoted by the points and the Standard Model prediction is shown in the open histogram. The acceptance constraints limit the effect of the radiation amplitude zero as well as the expected asymmetry.

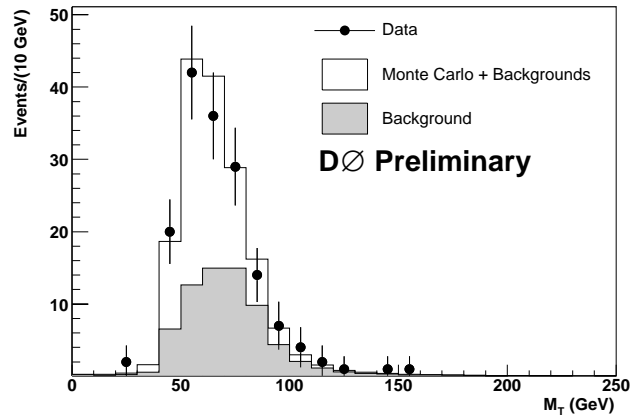


FIG. 6: Comparison of data (points), background (shaded histogram), and Monte Carlo + background (open histogram) for the transverse mass, M_T in muon channel.

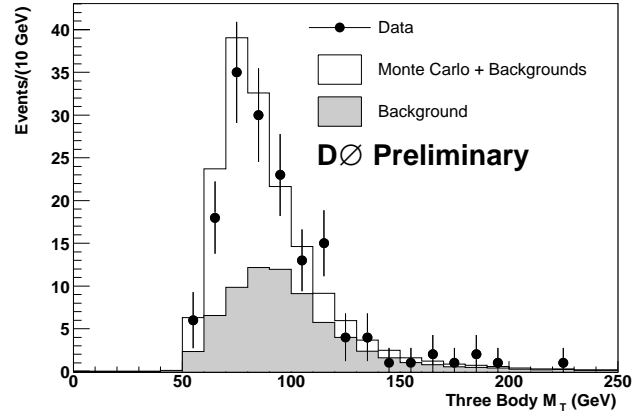


FIG. 7: Comparison of data (points), background (shaded histogram), and Monte Carlo + background (open histogram) for the three body ($\mu\nu\gamma$) transverse mass.

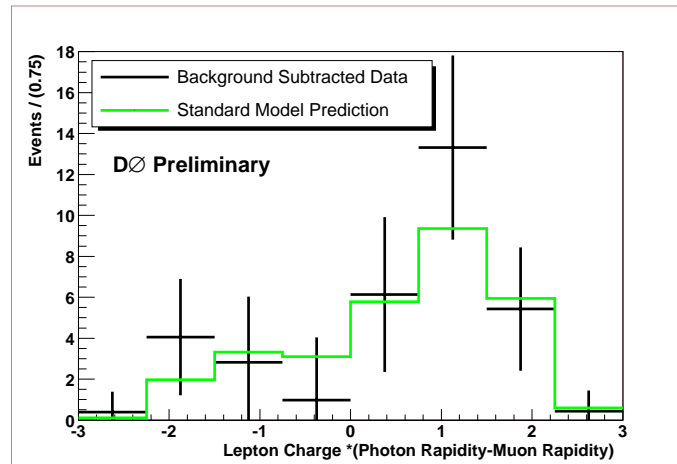


FIG. 8: Charge Signed Rapidity Difference in muon channel (background subtracted). Standard Model is shown for comparison.